CONFERENCE PRE-PRINT

ION DOPPLER SPECTROSCOPY SYSTEM ON THE SUNIST-2 SPHERICAL TOKAMAK

M.H. YANG[1], J.R. WANG[1], Y.P. QIN[1], B.B. WANG[2], S.Z. WANG[1], Y. TAN[2], and R. CHEN[1]
[1]Startorus Fusion, Xi'an, China
[2]Department of Engineering Physics, Tsinghua University, Beijing, China
Email: yangmenghua@startorus.cn

Abstract

An innovative Ion Doppler Spectroscopy (IDS) system with high spatial (every 22 mm on the radial plane) and temporal (2 ms) resolutions has been developed on SUNIST-2 (Sino-United Spherical Tokamak-2) for continuous measurement of the ion temperature profile. Through optimized optical design and a novel spectral fitting method based on the convolution of the complex instrument function, the Doppler broadening of the 529 nm CVI spectral line at specific points can be directly obtained, rather than being inferred from line-integrated measurements. The system successfully conducts continuous measurement of the ion temperature distribution across the entire midplane of the tokamak plasma during an experiment, and the experimental results indicate that the typical fitting errors of the system remain within 5% for typical spectrum and 15% when other strong impurity spectral lines are present in the range.

1. INTRODUCTION

The passive ion Doppler spectroscopy for ion temperature measurement addresses the spatial constraints inherent in compact conceptual devices, but there are still measurement challenges. Since the measured spectral line is line-integrated signal, the broadening of the line is influenced by both the ion temperature and the emission profile [1]. Howard [2], Balandin and Ono [3], and Tanabe [1] used the Abel inversion for tomographic reconstruction to solve the problem, obtaining 1D and 2D passive ion temperature profiles. However, tomographic reconstruction strongly depends on symmetry assumptions, and the spectral shape generated is more susceptible to noise, leading to significant reconstruction errors.

Furthermore, passive ion Doppler spectroscopy yields a spectrum that includes instrument broadening, Stark broadening, and Zeeman broadening [4], in which the instrument broadening (or instrument function) shows the predominant influence on the result and commonly assumed to be Gaussian distributed. Experimental results [5] show that instrument function often exhibits asymmetrical tailing. This leads to an overestimation of ion temperature when subtracting Gaussian-type instrument function, or even line distortion. A multi-Gaussian fitting method has been employed to improve the issue [5][6], but it has not entirely eliminated the impact.

The paper develops a novel IDS system to address the aforementioned issues, achieving more accurate and stable profiles of multichannel ion temperatures. Section 2 provides an overview of the system; Section 3 explains how the system obtains spectrum on the measurement points from line-integrated channels through optical design, physical analysis and data processing; Section 4 describes the newly developed deconvolution-based calibration method for complex instrument function, which address line distortion and ion temperature overestimation caused by tailing of the instrument function, and makes the measurement in Section 3 possible; Section 5 presents experimental results of this system on the SUNIST-2 spherical tokamak.

2. SETUP OF THE SYSTEM

The IDS system is applied to the SUNIST-2 spherical tokamak, whose major radius and minor radius are 525 mm and 325 mm, respectively. Its overall optical arrangement is similar to that of a CXRS system with vertically-incident neutral beam injection, as shown in FIG.1. The optical collection system consists of a collection lens and a parallel fibre bundle, focused on the mid-line of a poloidal cross-section. There are 36 available channels covering the radial line, with a spatial resolution of 22 mm and a temporal resolution of 2 ms. The collection lens is designed with a large aperture aspheric lens group (f=35 mm, F=1.4, with a filter diameter of 67 mm) to enhance the flux and reduce aberrations. The optical center of the lens is 1301 mm from the measurement plane, with respective near and far depth of field (DOF) being 20 mm and 30 mm. Each channel of the parallel fibre bundle (NA=0.22) has a core diameter of 400 μm and a cladding diameter of 600 μm. The fibres have a transmission distance of 32 m with a transmission loss less than 15% over the path, guiding the

light into an optical collection room shielded by lead walls to avoid interference from high-energy radiation on the CCD. The optical collection system is coupled to a monochromator (f=0.67 m, F=4.7, 1800 g/mm). The monochromator is connected to an ANDOR iXon Ultra 888 EMCCD, which has 1024×1024 pixels, each with a size of 13 μm×13 μm. The IDS system measures the 529 nm CVI line, with a linear dispersion of 0.62 nm/mm at the corresponding grating angle, equating to 0.008 nm/pixel on the EMCCD. The entrance of the monochromator adopts a three-slit configuration, with the fibre bundle reorganized into a 12×3 array to reduce aberrations and fully utilize the image of the CCD. Dummy fibres are used among channels to prevent crosstalk between adjacent active fibres. To ensure temporal resolution of continuous measurements, pixel binning by hardware is performed on the image of the CCD in the spatial direction of each fibre, resulting in an image output of 12×1024 (spatial axis × wavelength axis) per frame, as illustrated in FIG.2.

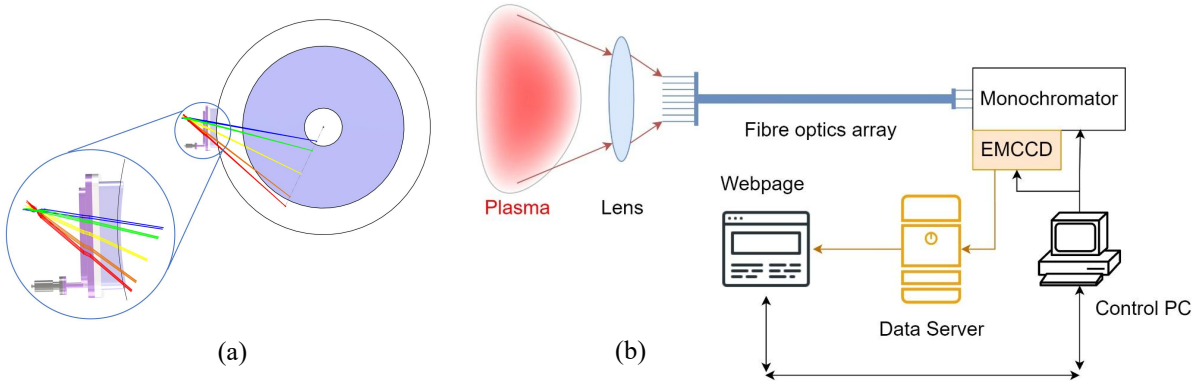

FIG. 1. (a) The optical collection arrangement of the system. (b) The schematic view of the system.

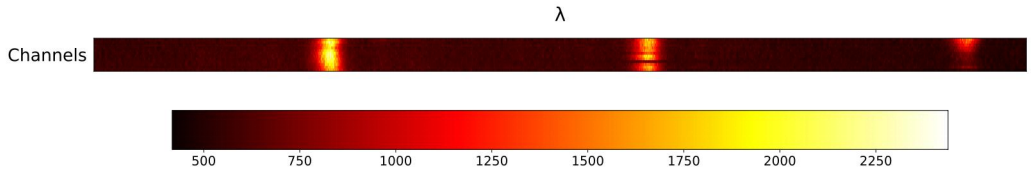

FIG. 2. A single frame of image output from the EMCCD. In the spatial axis (channels), hardware pixel binning combines 744 pixels into 12, each representing the spatial range of a channel along with its neighboring dummy fibres. In the wavelength axis, three distinct groups of peak regions can be observed, each corresponding to channels traversing one of the three slits, representing high-field side region, the core region, and the low-field side region, respectively.

3. DESIGN OF THE MEASUREMENT POINTS

For the collection lens with a fixed optical axis and image plane (where the parallel fibre bundle is located), its effective measuring range is a Gaussian beam-like region along the optical axis traversing the plasma, as shown in FIG.3(a). The beam diameter at the lens is consistent with the lens aperture, and the beam waist is located at the measurement plane (object plane). Light emitted by plasma closer to the object plane can be collected by the fiber bundle at a greater proportion on the image plane, and vice versa. Light emitted by plasma at the boundaries is dispersed over the image plane, with the proportion collected by the fiber bundle approaching zero. Thus, the light power collected by each channel of the parallel fibre bundle is approximately the sum of the light power from different region with weighting coefficients ε influenced by the numerical aperture of the fibre and the optical path design, where $\varepsilon \approx 1$ in the DOF region. At any given distance along the optical axis, the integral of the weighting coefficients over the cross-section perpendicular to the optical axis within the effective measurement range satisfies the following equation, where i and j denote two different arbitrary cross-sections:

$$\int \varepsilon_{i\perp} dl = \int \varepsilon_{j\perp} dl \quad (1)$$

The system minimizes the influence of dispersed light outside the DOF region on the measured spectral lines by data fitting method. Plasma rotation velocity differ at various radial positions, manifesting as frequency shift of the respective components in the measured spectral line. This effect can be illustrated in FIG.3(b) when the plasma rotation velocity becomes comparable to the thermal velocity of the ions. The spectral line can be divided into two parts: the red one represents the spectral line within the DOF, or the "measurement point"

where the ion temperature is assumed to be uniform — this is the ion temperature to be measured. The green components represent the influence of boundary, they symmetrically distributed along the wavelength axis due to the different frequency shifts caused by varying rotation velocity. All the green components combine into the blue component. Components within DOF and from boundary can be effectively separated using a dual Gaussian fit in practice, thereby obtaining the ion temperature of the "measurement point". The feasibility of this method requires further investigation when the plasma rotation velocity is much smaller than the ion thermal velocity.

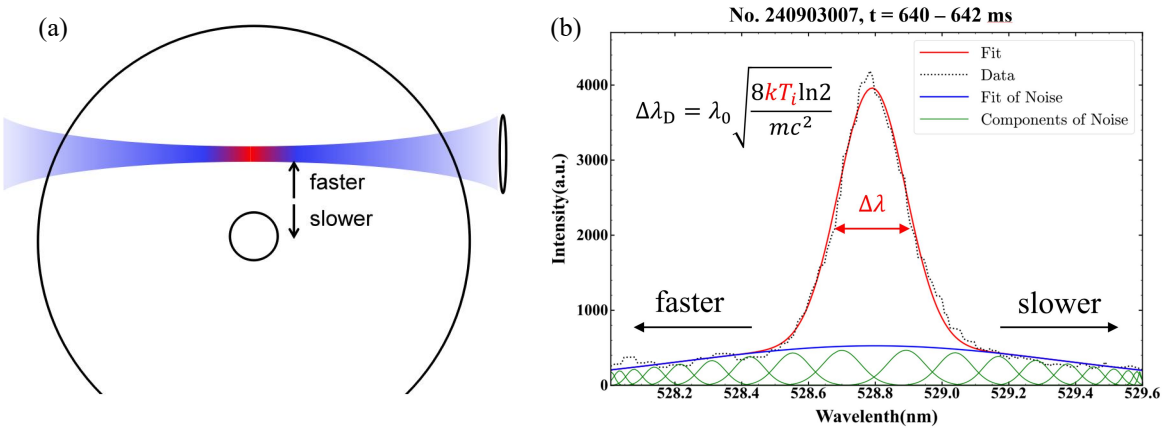

FIG. 3. (a) The effective measuring range of the collection lens, red within DOF and blue outside of DOF; (b) A schematic of the separated Doppler spectra for both internal and external DOF (with other noises). Due to the higher rotation velocity in the plasma core, the distribution is typically asymmetric.

4. COMPLEX INSTRUMENT FUNCTIONS CORRECTION

The prerequisite for separating the spectral components described in Section 3 is to obtain an accurate ion Doppler spectral line. In ion Doppler spectroscopy, the real Doppler broadening is often obscured by the instrument function. This phenomenon arises from instrumental effects due to various factors, including the grating, the entrance slit of the monochromator, the pixel size of the CCD, and the setup of the optical path [5]. The measured spectrum $g(\lambda)$ is thus the convolution of the real spectrum $f_0(\lambda)$ with the instrument function $h(\lambda)$:

$$g(\lambda) = \int f_0(\lambda')\, h(\lambda - \lambda')d\lambda' \tag{2}$$

The instrument function is typically assumed to follow a Gaussian distribution, thus Gaussian fitting and Wiener deconvolution [7] are employed to correct it. However, the real instrument function presents unidirectional asymmetric tails due to the grating angle and the slit width of the monochromator. Methods for Gaussian distribution may result in an overestimation of ion temperatures and failed fitting by severe spectral line distortion.

The work introduces an instrument function correction method based on an improved Richardson-Lucy iterative deconvolution algorithm. This approach effectively separates and corrects various asymmetric or complex instrument functions, exhibiting adaptive optimization capabilities. It enhances the reliability of ion temperature results and improves convergence speed relative to conventional deconvolution methods. For instrument function characterized by multi-Gaussian or Voigt functions, the measured spectrum can be expressed as:

$$g(\lambda) = f_0(\lambda) \otimes h(\lambda) + N(\lambda) \tag{3}$$

where $f_0(\lambda)$ is the real ion Doppler spectrum, and $N(\lambda)$ is the accumulated noise in measurements. The Richardson-Lucy iterative method [8][9] can be utilized for image denoising, optimizing the loss function based on the noise properties and the point spread function (PSF) of the system. The loss function $J(f)$ is given by:

$$\mathrm{J(f)} = \Sigma(\mathrm{f}^{(k)} \otimes \mathrm{PSF} - \mathrm{g}(\lambda) \cdot \ln(\mathrm{f}^{(k)} \otimes \mathrm{PSF})) \tag{4}$$

where $f^{(k)}$ is the estimated spectrum at the k-th iteration, with PSF representing the instrument function $h(\lambda)$. The deconvolution iteration formula for solving the spectrum can be derived:

$$\mathrm{f}^{(\mathrm{k}+1)} = \mathrm{f}^{(\mathrm{k})} * [(\frac{g(\lambda)}{f^{(k)} \otimes h(\lambda)}) \otimes \mathrm{h}(\lambda)^{\mathrm{T}}] \quad (5)$$

To address potential overfitting and false peak issues, the estimated spectrum obtained by the Richardson-Lucy algorithm needs regularization through physical constraints. The L2 norm of the second derivative is employed for Tikhonov regularization, with the objective function $O(f)$ expressed as:

$$\mathrm{O(f)} = \|\mathrm{f} \otimes \mathrm{h}(\lambda) - \mathrm{g}(\lambda)\|^2 + \alpha\left\|\nabla^2 \mathrm{f}\right\|^2 \quad (6)$$

where α is the regularization coefficient that can be adaptively optimized according to the signal-to-noise ratio (SNR) of the measured signal, satisfying:

$$\alpha = \alpha_0 * \mathrm{e}^{-\beta * \mathrm{SNR}} \quad (7)$$

Here, α_0 represents a pre-defined initialization value, where 0.05 has been experimentally determined as the most appropriate initial value. Furthermore, α decreases smoothly in an exponential manner as SNR increases. β is the decay coefficient controlling the influence of SNR fluctuations (default 0.1). When SNR is high, a smaller α can retain more spectral details; when SNR is low, increasing α helps suppress noise through the smoothing effect of regularization.

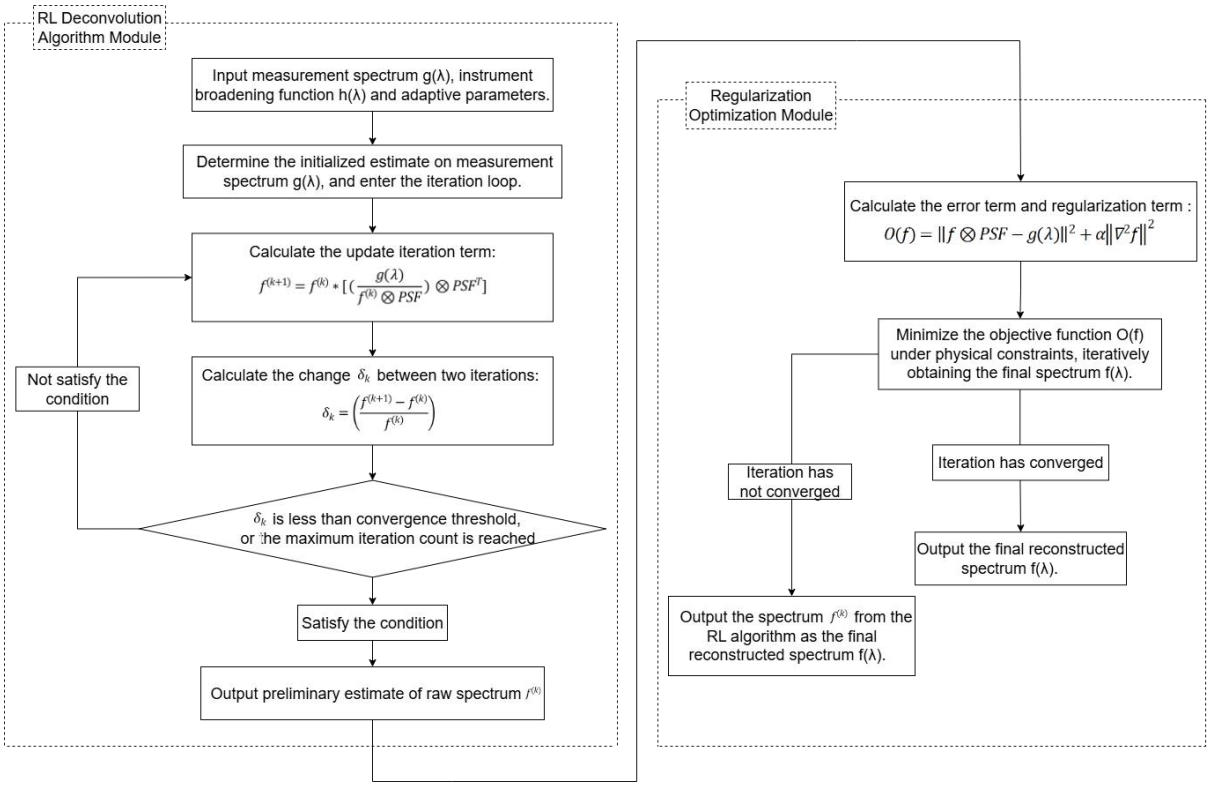

FIG. 4. The entire calculation process for correction of complex instrument functions.

FIG.4 and FIG.5 illustrate the entire calculation process and the result of the correction method in the section, respectively. FIG.5(a) presents a typical result of the correction method. The red solid line represents the measured spectrum $g(\lambda)$. Given a known and calibrated instrument function $h(\lambda)$, the real spectrum $f_0(\lambda)$—shown as the black solid line—can be retrieved. A Gaussian fit is then applied to the real spectrum, yielding the cyan solid line, which is used for subsequent ion temperature calculations. To validate the consistency between the calculated ion temperature and the measured spectrum, the fitted Gaussian distribution is convolved with $h(\lambda)$ to reconstruct $g(\lambda)$, shown as the blue dashed line. The reconstructed $g(\lambda)$ shows excellent agreement

with the original one, with a root-mean-square error of less than 3%. This method also proves effective in handling cases where other impurity lines (typically Fe III lines) are present, as illustrated in FIG.5(b). The deconvolved real spectrum clearly reveals two Gaussian peaks. A dual-Gaussian fitting approach can effectively separate the C VI line from the other impurity line, and the root-mean-square error of the reconstructed g(λ) is around 14%.

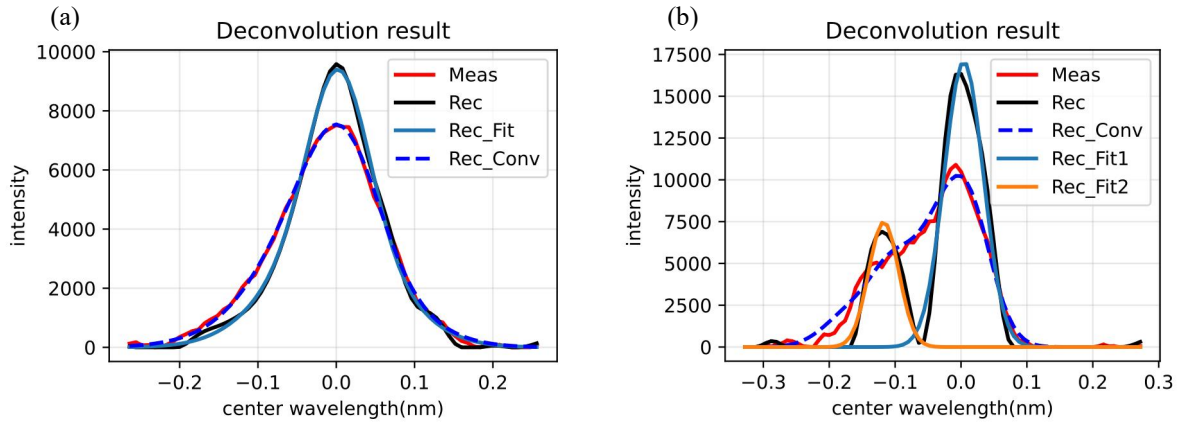

FIG. 5. Results of the instrument function correction, including the fitting of the deconvolved spectrum and validation against the measured spectrum. (a) A typical result; (b) Results in the presence of additional impurity spectral lines.

5. EXPERIMENTAL RESULTS

Through the processes outlined, the system enables the acquisition of high-resolution ion Doppler spectroscopy data from SUNIST-2. Notably, the system encounters significant noise issues in measurements involving high-parameter plasmas, consisting of shot noise, CCD readout noise, and high-energy radiation. Despite the CCD being shielded, substantial interference from high-energy radiations still observed, particularly during disruptions. For tomographic reconstruction of the chord-integrated IDS system, the reconstruction process is sensitive to noise, resulting in considerable reconstruction errors. Additionally, toroidal rotation and the application of smoothing can also influence errors [1]. Conversely, for IDS system in the paper, the impact of noise is manageable. It can be assessed through pre-fitting, and corrected via standard procedures such as smoothing, baseline correction, and outlier filtering, which are not elaborated upon here.

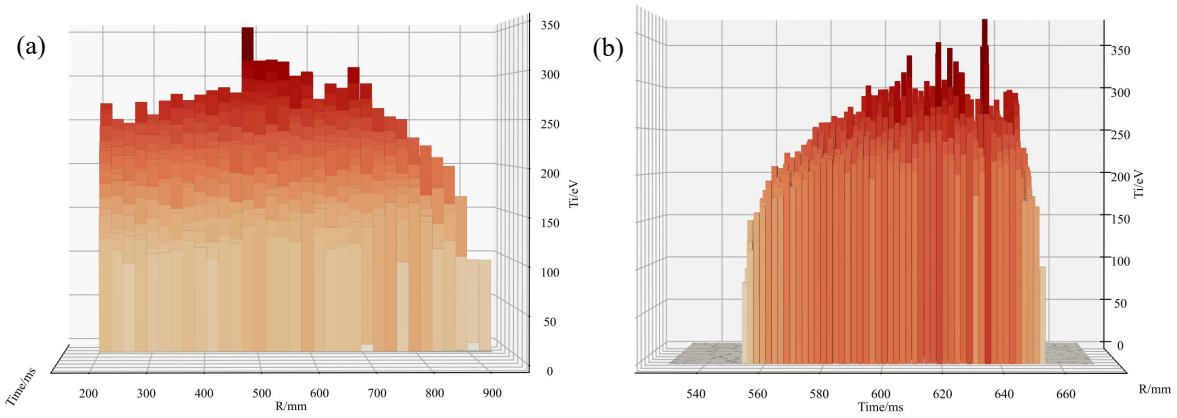

FIG. 6. The time evolution of the ion temperature radial profile for time shot #240828015 on the SUNIST-2. (a) Profile from spatial perspective; (b) Profile from temporal perspective.

As shown in the FIG.6, the IDS system obtains the temporal evolution of the ion temperature radial profile for time shot 240828015 on the SUNIST-2. The shot utilized a combination of merging-compression coils and the central solenoid coil for ohmic discharge, achieving a plasma current I_p around 200 kA and a line-averaged electron density n_e of $1 \times 10^{19} \mathrm{m}^{-3}$. The 36 measurement points, spaced 22 mm apart, cover the mid-line of the plasma poloidal cross-section. The frame interval for the measurements is 2 ms, with each frame having an

exposure time of 1.4 ms. From the spatial perspective, the radial profile of ion temperature reveals a larger gradient at the low-field side boundary, and the measured temperature on the high-field side exceeding that of the low-field side. This discrepancy might be due to radiation from sputtered impurities of the central column. From the temporal perspective, the ion temperature continues to rise under the influence of the toroidal electric field until a disruption occurs.

6. CONCLUSION

The work has developed a novel IDS system to mitigate the reconstruction errors caused by various types of noise in tomographic measurement systems and to address the common problem of complex instrument functions in spectral line measurements. As a result, the system provides more accurate and stable multi-channel ion temperature radial profiles and their temporal evolution. Implemented on the SUNIST-2 spherical tokamak, it suppresses the contribution of regions out of DOF to the measured spectral lines through data fitting, effectively creating "measurement points" in engineering terms. The system features 36 effective radial channels covering the mid-line of a poloidal cross-section, with a spatial resolution of 22 mm, a frame interval of 2 ms, and a frame exposure time of 1.4 ms. By employing an instrument function correction method based on an improved Richardson-Lucy iterative deconvolution algorithm, more precise ion Doppler spectrum can be obtained, with fitting errors of approximately 3%. Even in cases where other impurity spectral lines interfere, the fitting error remains below 15%.

ACKNOWLEDGEMENTS

The work is supported by the Startorus Fusion. Deeply thanks to the SUNIST-2 group for providing the necessary resources and technical assistance for the study.

REFERENCES

[1] Tanabe, H., et al. "Two-dimensional ion temperature measurement by application of tomographic reconstruction to Doppler spectroscopy." *Nuclear Fusion* 53.9 (2013): 093027.

[2] Howard, John. "Vector tomography applications in plasma diagnostics." *Plasma physics and controlled fusion* 38.4 (1996): 489.

[3] Balandin, A. L., and Y. Ono. "Tomographic determination of plasma velocity with the use of ion Doppler spectroscopy." *The European Physical Journal D-Atomic, Molecular, Optical and Plasma Physics* 17.3 (2001): 337-344.

[4] Kunze, Hans-Joachim. *Introduction to plasma spectroscopy*. Vol. 56. Springer Science & Business Media, 2009.

[5] Fu, Jia. "The Basic Behaviors of Plasma Impurities and the Argon Transport of Plasma Impurities on the EAST Tokamak." PhD dissertation. University of Chinese Academy of Sciences, 2011.

[6] Xiong, Yanwei. "Data analysis and study of impurity particles behavior on EAST advanced optical diagnostics." MA thesis. University of Chinese Academy of Sciences, 2013.

[7] Zou, M. Y. "Deconvolution and signal recovery." *National defence industry press*, Beijing (2001): 78.

[8] Richardson, William H. "Bayesian-Based Iterative Method of Image Restoration." *Journal of the Optical Society of America*, vol. 62, no. 1, Jan. 1972, pp. 55-59.

[9] Lucy, L. B. "An Iterative Technique for the Rectification of Observed Distributions." *The Astronomical Journal*, vol. 79, no. 6, June 1974, pp. 745-754.